$B(4,4) = 2\pi^2\Delta t^2$ (Yamamoto *et al.*, 1984). No simple model was found allowing the explanation of the nearly linear increase of the phase fluctuation with A_{max}.

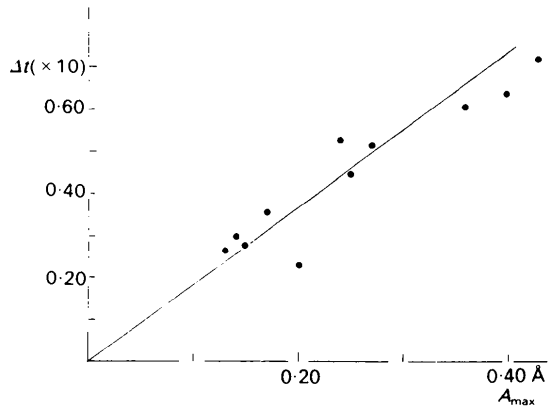

Fig. 10. The correlation between Δt ($\times$ 10) and A_{max}; Δt is related to the phase fluctuation $\Delta\varphi = 2\pi\Delta t$ occurring for the modulation wave of an atom and A_{max} is the largest displacement of the latter.

The authors thank Drs D. Grebille and A. Leclaire for helpful discussions and Mrs J. Chardon for technical assistance.

References

B. A. FRENZ & ASSOCIATES, INC. (1982). *SDP Structure Determination Package*. College Station, Texas, USA.
DOUDIN, B. (1985). Private communication.
DURIF, A. & AVERBUCH-POUCHOT, M. T. (1982). *Acta Cryst.* B**38**, 2883–2885.
PETŘÍČEK, V. & COPPENS, P. (1985). *Acta Cryst.* A**41**, 478–483.
RIOU, D., LABBE, P. & GOREAUD, M. (1988*a*). *C. R. Acad. Sci.* **307**, 1751–1756.
RIOU, D., LABBE, P. & GOREAUD, M. (1988*b*). *C. R. Acad. Sci.* **307**, 903–907.
WOLFF, P. M. DE, JANSSEN, T. & JANNER, A. (1981). *Acta Cryst.* A**37**, 625–636.
YAMAMOTO, A. (1982*a*). *REMOS*. A computer program for the refinement of modulated structures. National Institute for Research in Inorganic Materials, Niiharigun, Ibaraki, Japan.
YAMAMOTO, A. (1982*b*). *Acta Cryst.* A**38**, 87–92.
YAMAMOTO, A., NAKAZAWA, H., KITAMURA, M. & MORIMOTO, N. (1984). *Acta Cryst.* B**40**, 228–237.
ZUÑIGA, F. J., MADARIAGA, G., PACIOREK, W. A., PÉREZ-MATO, J. M., EZPELETA, J. M. & ETXEBARRIA, I. (1989). *Acta Cryst.* B**45**, 566–576.

Acta Cryst. (1991). B**47**, 617–630

Structures and Transformation Mechanisms of the η, γ and θ Transition Aluminas

BY RONG-SHENG ZHOU* AND ROBERT L. SNYDER†

Institute for Ceramic Superconductivity, New York State College of Ceramics, Alfred University, Alfred, NY 14802, *USA*

(*Received* 1 *October* 1990; *accepted* 27 *February* 1991)

Abstract

The defect crystal structures of η-, γ- and θ-alumina obtained from dehydroxylation of well crystallized bayerite and boehmite have been derived from the analysis of their X-ray powder diffraction patterns and from the Rietveld refinement of their neutron powder diffraction patterns. Profile analysis of the various reflection zones in these defect spinel structures shows different coherent domain sizes which can be associated with the tetrahedral and octahedral aluminium and the oxygen sublattices. These observations have been used to define the nature of the crystal structures, and to give insight into the transformation mechanisms. The very large surface energies of these phases are evident in the observation of a nearly three-coordinated surface Al atom in the η phase, and are the reason for the stability of the defect spinel structures of the transition aluminas. The reduction of surface area and the ordering of the tetrahedral Al sublattice which occurs on heating causes the spinel framework to collapse so that the structure, which exhibits tetragonal character at the early stage of the transition, settles into monoclinic θ-alumina *displacively* at the later stage, and eventually transforms to hexagonal corundum *reconstructively*. Thus θ-alumina should be considered the ultimate rather than the intermediate structural form into which the transition aluminas could evolve on the way to corundum. The overall crystal structure of the transition aluminas should therefore be viewed intrinsically as *spinel deformed* rather than as *tetragonally deformed*. Crystal data at room temperature: η-alumina, cubic, $Fd3m$, $a = 7{\cdot}914\ (2)$ Å, $R_B = 6{\cdot}24$, $R_p = 6{\cdot}50$, $R_w = 8{\cdot}43\%$; γ-alumina, cubic, $Fd3m$, $a =$

* Present address: Materials Data, Inc., PO Box 791, Livermore, CA 94550, USA.
† To whom all correspondence should be directed.

0108-7681/91/050617-14$03.00

7·911 (2) Å, $R_B = 10{\cdot}53$, $R_p = 7{\cdot}61$, $R_w = 10{\cdot}25\%$; θ-alumina, monoclinic, $C2/m$, $a = 11{\cdot}854$ (5), $b = 2{\cdot}904$ (1), $c = 5{\cdot}622$ Å, $\beta = 103{\cdot}83$ (7)°, $R_B = 15{\cdot}02$, $R_p = 9{\cdot}37$, $R_w = 11{\cdot}93\%$.

Introduction

The transition aluminas refer to the group of partially dehydrated aluminium hydroxides other than anhydrous α-alumina (corundum) as illustrated in Fig. 1 (Wefers & Misra, 1987). The temperature ranges of stability for the transition aluminas are approximate. They depend, among other things, upon the crystallinity and impurities of the starting materials and the thermal treatment. All the transition aluminas are reproducible and stable at room temperature, but the sequence of transformation is not reversible with decreasing temperature. Therefore they should be called transition forms rather than different phases of aluminium oxide. We will, however, continue the universal practice of referring to them by their common name 'Greek letter'-aluminas. The diffuse characteristic of the powder patterns reflects a high degree of structural disorder in the transition aluminas (see Figs. 2 and 3), but the similarity of the patterns may indicate certain structural aspects that pervade all these phases.

The transition aluminas are widely used in industry as adsorbents, catalysts or catalyst carriers, coatings and soft abrasives because of their fine particle size, high surface area and the catalytic activities of their surfaces. These remarkable properties have induced a great deal of scientific curiosity about their structures. Extensive research has been carried out over the past few decades studying and characterizing the transition aluminas with respect to dehydroxylation and the transformation mechanism, porosity and specific surface area, surface structure and chemical reactivity, and the defect crystal structure [see Wefers & Misra (1987) for an excellent review]. However, the poor crystallinity and possible surface-energy stabilization has made it impossible for advanced surface analytical techniques to probe such fine and irregular surfaces, and for detailed single-crystal diffraction study of the poorly ordered structures.

This study focuses on the most disordered and least understood defect crystal structures of the transition aluminas which were derived from well crystallized powder samples of aluminium trihydroxide (bayerite) and monohydroxide (boehmite). The two sequences of decomposition are similar, producing the η- and γ-alumina phases, which are the most widely used forms of the transition aluminas.

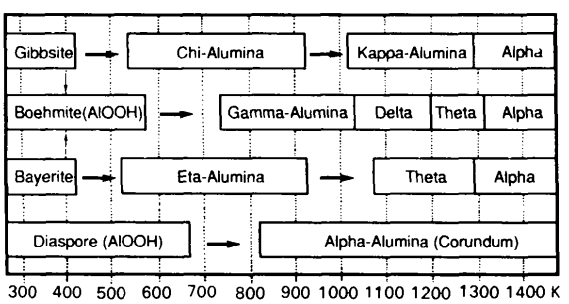

Fig. 1. Thermal diagram of the transition aluminas (after Wefers & Misra, 1987).

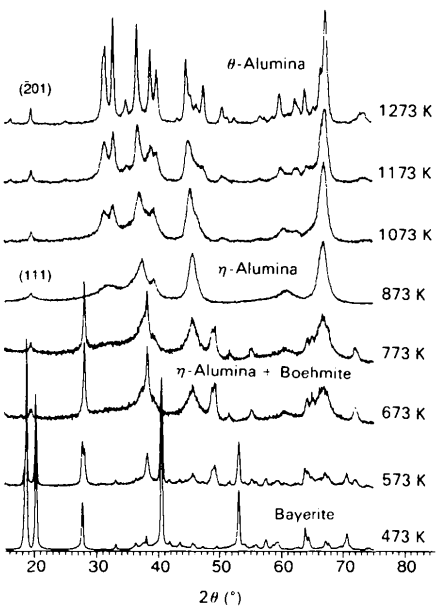

Fig. 2. XRD powder patterns of bayerite and its derivatives.

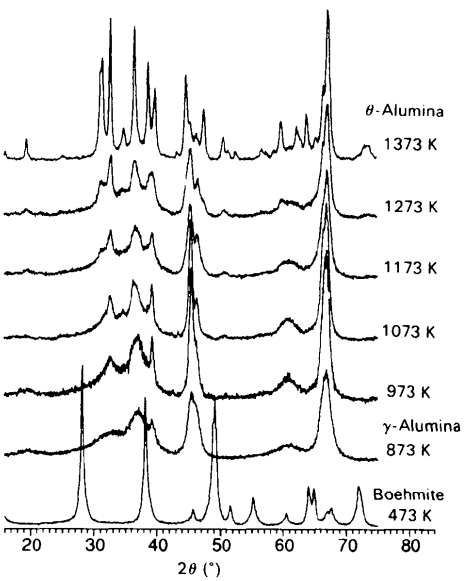

Fig. 3. XRD powder patterns of boehmite and its derivatives.

Dehydroxylation of boehmite and bayerite

Goton (1955) reported the heating of well crystallized boehmite at a rate of 4·5 K min^{-1} to produce a strong endothermic effect at 780 K. The specific surface area increases to < 100 m^2 g^{-1}, and a transition alumina called γ forms. Goton's results agree well with the findings of Lippens (1961) who investigated the dehydroxylation of well crystallized and gelatinous boehmite. The latter materials developed high-surface-area transition aluminas similar to those formed in the dehydroxylation of bayerite. The well crystallized boehmite decomposed to γ, then formed θ, which was followed by α. The gelatinous form converted to η, then *via* θ to α.

An important phenomenon in the dehydroxylation of aluminium hydroxides is that the transformations are pseudomorphic: the external shape of the hydroxide crystal remains and there is an orientation relationship of the lattice axes of the new structure to those of the original. Lippens (1961) and Wefers & Misra (1987) among others, showed by transmission electron microscopy (TEM) that the hydroxide particle loses transparency and smoothness upon heating and a sponge-like texture develops within a coherent solid. Parallel pores located in the cleavage plane (001) separate the solid into fine lamellae that are about 20 Å thick. A network of irregularly shaped slits, about 10 Å wide, intersect and divide the lamellae into interconnected irregularly shaped solid domains which measure, on average, less than 100 Å in their longest dimension. Surface areas resulting from this pore system can easily exceed 300 m^2 g^{-1} (Wefers & Misra, 1987) and the majority of the new surfaces come from the (111) crystallographic plane of the resulting spinel-type lattices of η- and γ-alumina.

Lippens & DeBoer (1964) assumed, in view of the lamellar texture, that the cubic close-packed oxygen layers in the η structure are one-dimensionally disordered in the direction parallel to the c axis of the precursor bayerite (which is the [111] direction of the spinel). Ervin (1952) observed that the X-ray powder diffraction patterns of all the transition aluminas have in common the strong line at $d = 1{\cdot}39$ Å ($2\theta = 67{\cdot}3°$), see Figs. 2 and 3 (all 2θ's refer to Cu $K\alpha_1$ radiation). This reflection belongs to the (440) plane of the spinel structure, for which all the oxygen ions and all of the possible Al ions, both tetrahedral or octahedral, scatter in phase. The less-intense (400) plane of the spinel at about $d = 1{\cdot}99$ Å ($2\theta = 45{\cdot}5°$) has all of the anions but only the octahedral cations scattering in phase. On this basis, we can observe that all the transition aluminas have oxygen ions in approximately cubic close packing. The differences in their patterns represent changes in intensities of reflections resulting from differences in the distribution of the Al ions. The initial cation disorder of the low-temperature forms depends upon the precursor used. The phases become more ordered with increasing heat treatment.

Crystal structures of η-, γ- and θ-alumina

As described above, both, η- and γ-alumina have a spinel-type structure. Stumpf, Russell, Newsome & Tucker (1950) determined the cubic lattice constant of η-alumina to be 7·9 Å. Lippens & DeBoer (1964) found, by selected-area electron diffraction, that η-alumina is somewhat tetragonally deformed with the c/a ratio varying between 0·985 and 0·993, and γ-alumina is more tetragonally deformed with the c/a ratio varying between 0·983 and 0·987, but that the oxygen sublattice of γ-alumina is fairly well ordered, much more so than that of η-alumina. The strong anisotropy of the shrinkage in the a and b axes of boehmite, they believed, is the cause of the more pronounced tetragonal character of γ-alumina. According to Yamaguchi, Yanagida & Ono (1964), however, the degree of tetragonal deformation is a function of the residual content of hydroxyl ions. The reason for the difference in the two spinel-type structures likely lies in the structures of the precursors. Bayerite is made up of weak hydrogen-bonded single layers of $Al(OH)_6$ octahedra (Zigan, Joswig & Burger, 1978), which lose half of their oxygen ions on dehydroxylation. In boehmite, however, the double layers of $Al(OH)_6$ octahedra are strongly hydrogen bonded and already have oxygen ions in quasi-cubic close-packing (Hill, 1981). Only a quarter of the oxygen ions are driven off in the dehydroxylation of boehmite.

In the normal $M^{3+}M^{2+}$ (AB_2O_4) spinel, 32 oxygen anions and 24 cations make up the unit cell. However, only $21\frac{1}{3}$ Al^{3+} ions are available for the cation positions in η-alumina and in the isomorphic γ-alumina. Thus, the spinel-type lattice of η- and γ-alumina contains cation vacancies. Since the Al ion favors octahedral coordination under normal circumstances, Saalfeld & Mehrotra (1965) assumed all octahedral sites to be occupied, the cation vacancies being confined to the tetrahedral sites.

Since η- and γ-alumina contain residual hydroxyl ions, DeBoer & Houben (1952) believed them to be hydrogen spinels, analogous to the lithium spinel described by Kordes (1935). Soled (1983) postulated that the hydroxyl ions are a necessary component of the defect structure of η- and γ-alumina, their number being equal to the number of cation vacancies.

Shirasuka, Yanagida & Yamaguchi (1976) prepared η-alumina from a plasma-coated alumina balloon on a Pt substrate and refined the η structure from its X-ray powder diffraction pattern in space

group $Fd\bar{3}m$, with an ideal spinel oxygen sublattice, to give a cubic cell of $a = 7{\cdot}906\,(1)$ Å. They found that 62·5% of the Al ions occupy two 16-fold [16(*c*) and 16(*d*)] octahedral sites and assumed the remaining Al ions to be distributed equally over the 8-fold and the 48-fold tetrahedral sites.

John, Alma & Hays (1983) used solid-state NMR with magic angle spinning to determine the coordination of Al ions in the transition aluminas. They found 65 (4) and 75 (4)% of the Al ions in the octahedral sites in η- and γ-alumina respectively. The η-alumina results agree well with Shirasuka's. The cation vacancies therefore appear to favor octahedral sites in η-alumina but tetrahedral sites in γ-alumina. The same workers showed that in θ-alumina prepared from both bayerite and boehmite, the Al ions were almost exclusively in octahedral coordination. This is in contrast to Saalfeld's (1960) and Yamaguchi, Yasui & Chiu's (1970) structure analyses of θ-alumina in which both assumed half of the Al ions were occupying the tetrahedral sites based on the known structure of isomorphic β-Ge_2O_3 which can be grown in large single crystals. Wefers & Misra (1987) considered the θ structure an intermediate between the cubic close packing of the low-temperature transition aluminas and the hexagonally close-packed corundum.

Experimental and results

Sample preparation and data collection

Both hydrogen and deuterated samples of bayerite used in this study were furnished by Alcoa. XRD scans (Fig. 2) showed the samples to be well crystallized single-phase bayerite. The hydrogen sample of boehmite was prepared by mixing fine and pure powder of metallic aluminium with distilled water in stoichiometric ratios and heating it to 473K in a hydrothermal bomb for 12h. The deuterated sample of boehmite was prepared in the same way except for replacing distilled water by pure heavy water (100 at% D). The resulting products are fine white powders. XRD analysis (Fig. 3) confirmed that they are well crystallized single-phase boehmite.

IR analysis performed on a Nicolet 60 SXR FT-IR spectrometer showed that the deuteration is better than 50% for both deuterated boehmite and bayerite. Differential thermal analysis (DTA) data (Fig. 4) were collected on a DuPont 9900 thermal analyzer with a load of 25 mg and a heating rate of 20 K min^{-1}. XRD scans (Figs. 2 and 3) were also taken from progressive heat treatment of bayerite and boehmite at elevated temperatures.

The DTA clearly shows the presence of a trace of boehmite in the dehydroxylation products of bayerite in the temperature region corresponding to the first endothermic peak of bayerite. Therefore, the third endothermic peak of bayerite, around 773 K, must result from the decomposition of boehmite to γ-alumina. Consequently, η-alumina obtained from the dehydroxylation of bayerite inevitably contains a very small amount of γ-alumina which confirms the finding of Lippens & DeBoer (1964). Notice that no significant thermal activity is observed in the DTA around 1273 K where the transition from both η- and γ- to θ-alumina takes place.

The X-ray samples of η-, γ- and θ-alumina were obtained from a one-shot (*i.e.* direct insertion of the sample into a preheated furnace) calcination of the hydrogen-containing samples of bayerite at 873 K, boehmite at 873 K and bayerite at 1273 K in air for 8 h respectively. Their XRD powder patterns (Figs. 5 and 6) were collected at room temperature on a Siemens Diffrac-500 diffractometer, equipped with a Cu target X-ray tube and a diffracted-beam graphite

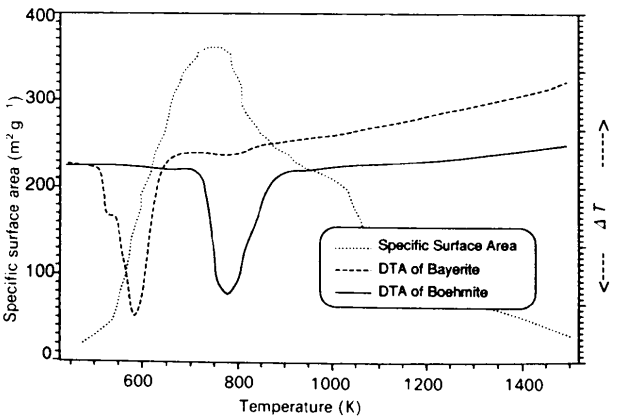

Fig. 4. DTA data of bayerite and boehmite [specific surface area data from Wefers & Misra (1987)].

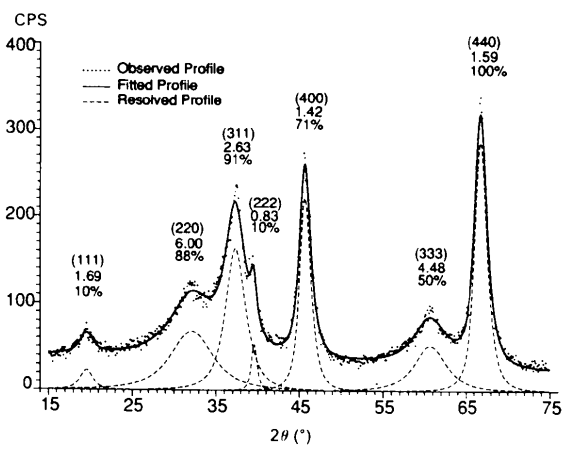

Fig. 5. Profile fit of XRD powder pattern of η-alumina. Values given above the peaks are *hkl*'s, FWHM and relative intensity.

monochromator, with a step size of 0·05° 2θ and a count time 5 s.

The neutron samples of η-, γ- and θ-alumina were obtained from a one-shot calcination of the deuterated samples of bayerite at 873 K, boehmite at 873 K and bayerite at 1273 K in air for 8 h respectively. Their neutron powder diffraction patterns (Fig. 7) were collected at room temperature, on a five-detector diffractometer apparatus with a monochromatized thermal neutron source (λ = 1·548 Å) at the National Institute of Standards and Technology, with a step size 0·05° 2θ and the sample sealed in a vanadium tube. Platinum crucibles were used in the preparation of both the X-ray and neutron samples of η-, γ- and θ-alumina.

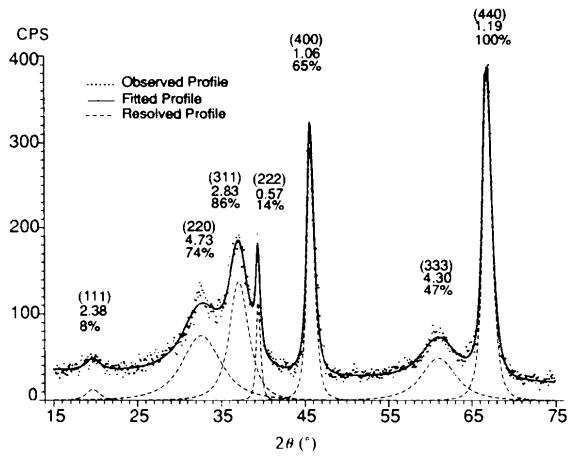

Fig. 6. Profile fit of XRD powder pattern of γ-alumina. Values given above the peaks are *hkl*'s, FWHM and relative intensity.

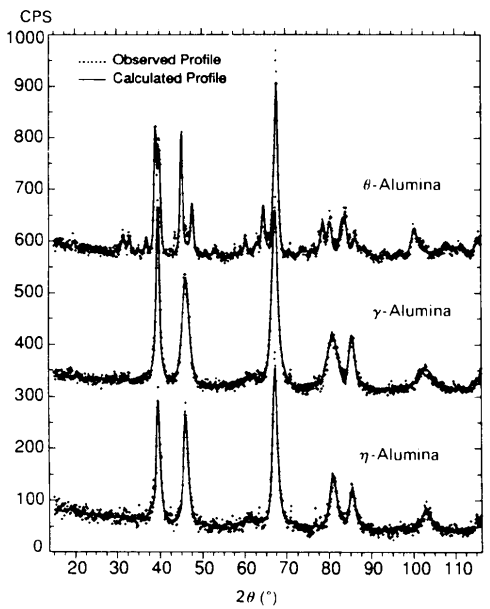

Fig. 7. Neutron profile refinement of η-, γ- and θ-alumina.

Table 1. *Loss-on-ignition analysis of η-, γ- and θ-alumina*

Form	wt%	x in $Al_2O_3.xH_2O$	(OH) per unit cell
η	1·00 (5)	0·057 (3)	1·19 (5)
γ	0·84 (5)	0·048 (3)	1·00 (5)
θ	0·10 (5)	0·006 (3)	0·05 (2)

Hydrogen content

To find out exactly how many residual hydroxyl ions the transition aluminas contain, one-shot loss-on-ignition analysis was carried out on the hydrogen samples of η-, γ- and θ-alumina in the following way: nine samples of about 10 g each, from each of the three aluminas, were calcined in corundum crucibles at 873 K for 1 h to drive off the surface adsorbed water, allowed to cool in an desiccator, and then weighed on an electronic balance to a precision ±1 mg. The same procedure was repeated for the same samples calcined at 1473 K for 6 h to drive off the residual hydroxyl ions. XRD scans confirmed that all nine samples had been converted to corundum. The results are given in Table 1.

The values in Table 1 are much smaller than those obtained from conventional thermogravimetric analysis (TGA) reported by previous workers (*e.g.* Wefers & Misra, 1987), which are in the range of a few weight percent. Previous numbers derived from a TGA curve were likely overestimated because of the difficulty in correcting for TGA instrumental baseline drifts. The hydrogen spinel postulated by DeBoer & Houben (1952) for η- and γ-alumina can thus be ruled out. It is also unlikely that one hydroxyl ion per spinel unit cell would have a significant effect on the observed tetragonal deformation of γ-alumina as suggested by Yamaguchi & Yanagida (1964) and on the transition of η- and γ- to θ-alumina.

Profile analysis of the XRD powder patterns

As can be seen in Figs. 2 and 3, both XRD and neutron powder patterns of η- and γ-alumina are very diffuse and exhibit extensive reflection overlapping. The differences in relative reflection intensities between the XRD and neutron patterns are largely the result of the differences in Lp and atomic scattering factors. Therefore, the XRD patterns manifest more scattering from Al sublattices, especially at low angle, whereas the neutron patterns are dominated by scattering from the oxygen sublattice.

Since reflection broadening in this strain-free system is directly related to lattice disorder and crystallite size, a quantitative estimate of the

broadening is essential for this study and was accomplished by profile fitting of the whole XRD patterns. The computer program *SHADOW* (Howard & Snyder, 1985, 1989) was used to deconvolute the specimen broadening function for the different crystallographic zones. By trial and error, a symmetric intermediate Lorentzian profile function was found to best describe the XRD powder patterns of η- and γ-alumina. The results are illustrated in Figs. 5 and 6, where the patterns are indexed based on a spinel cell in space group *Fd3m* and the values of the full width at half maximum (FWHM) of individual reflections are listed together with their *hkl*'s and relative intensities.

A typical pattern exhibits normal reflection broadening as a function of 2θ scanning angle in a smooth manner, being caused mainly by instrumental factors at low angles and dominated by wavelength dispersion at high angles. The XRD powder patterns of η- and γ-alumina exhibit *anomalous* reflection broadening in two aspects: (*a*) irregular broadening among peaks of different *hkl*'s (even from the same crystal zone) and (*b*) the formation of an odd peak shape with broadened base and sharp top that cannot be fit well by a single profile function. The first aspect is best illustrated by the broadening of the (111), (222) and (333) reflections from the same crystal zone, and the second aspect by the (111) and (311) reflections.

The high-quality diffraction data shown in Figs. 2 and 3 allows one to recognize that the subtle differences in the XRD powder patterns of η- and γ-alumina lie in: (*a*) the absence of a sharp (111) reflection in γ, (*b*) a slight splitting, or obvious shoulder, of the (400) reflection of γ, and (*c*) a shift of the (311) and (220) reflections of γ to lower angle. The latter two differences can be accounted for by a more pronounced tetragonal deformation of γ-alumina over that seen in η-alumina. We conclude that the strong asymmetric nature of the (311) and (220) reflections routinely observed in η-alumina, and forced to ones attention while profile fitting, is caused by the presence of a trace amount of γ-alumina in η-alumina as revealed from the DTA analysis and does not reflect an intrinsic property of the material. As will be shown, this is another way of saying that there are two different ordering lengths of the Al ions on the tetrahedral sites.

With the pseudomorphosis of the dehydroxylation in mind, profile fitting was also performed on the XRD powder patterns of the precursor bayerite and boehmite samples as well as those of the derived θ- and α-alumina. Notice that these powder patterns (Figs. 2 and 3) do not show the anomalous broadening seen in η- and γ-alumina. Their average crystallite sizes can therefore be estimated from the FWHM of the specimen broadening convolute of any single non-overlapping reflection according to the Scherrer (1918) formula where the average crystallite size (or ordering domain) is

$$t = \lambda/B\cos(\theta_b)$$

where t is size of ordering domain, λ the diffraction wavelength, B the integral breadth of the specimen convolute, and θ_b the Bragg angle of reflection. B is obtained from the observed FWHM by deconvoluting a Lorentzian profile, which models the specimen broadening (S), with a profile which models the instrumental (G) and wavelength (W) convolutes $W*G$. The $W*G$ function is obtained by careful calibration of the diffractometer with a standard which has no size, defect or strain broadening. In this study, an NBS standard reference material (SRM640A, silicon powder) was used which exhibits only a small amount of size broadening that will cause a trivial error in the size estimates reported (Howard & Snyder, 1989). The results are 410 (10) Å for bayerite, 150 (10) Å for boehmite, 230 (10) Å for θ-alumina and 630 (10) Å for α-alumina.

With this quantitative information on reflection broadening in mind, ideal XRD powder patterns were calculated using ideal spinel sublattices and compared with the observed pattern of γ-alumina. Constant FWHM, isotropic temperature factors, full site occupancy and a spinel cell of $a = 7{\cdot}9$ Å were used in these calculations. In an ideal spinel lattice in space group *Fd3m*, cubic close-packed oxygen ions are in the 32(*e*) site (see Fig. 8). Octahedral Al ions could be in the 16(*d*) and/or in the 16(*c*) sites. Tetrahedral Al ions could be in the 8(*a*) and/or in the 8(*b*) and/or in the 48(*f*) sites; the latter would necessarily be poorly occupied if at all. The computations are illustrated in Fig. 9. The following structural information can be extracted from the above profile and pattern calculations provided the space group of the structure is *Fd3m*:

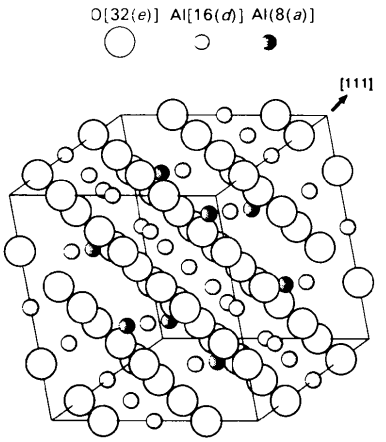

Fig. 8. Spinel unit cell with O and Al sublattices.

(*a*) The oxygen sublattice in both η- and γ-alumina is fairly well ordered as discovered by Lippens & DeBoer (1964) because the sharp (222) reflection is dominated by the scattering from the oxygen sublattice. The ordering domain of the oxygen sublattice estimated from the FWHM value of the specimen convolute S of the (222) reflection is 98 (2) Å for η-alumina and 200 (10) Å for γ-alumina. These numbers are comparable with the average crystallite sizes of the precursor bayerite and boehmite. In fact the η value agrees well with the average long dimension of its dehydroxylated lamellae as observed by TEM. Thus, it is the framework of close-packed oxygens which supports the original crystallite shape and accounts for the pseudomorphosis of dehydroxylation.

(*b*) Both η- and γ-alumina have octahedral Al as well as tetrahedral Al ions since the (220) reflection is only due to scattering from the tetrahedral Al sublattice.

(*c*) The tetrahedral Al sublattices in both η- and γ-alumina are very disordered because the (220) reflection is the most diffuse in the pattern. The ordering domain of the tetrahedral Al sublattice estimated from the FWHM value of S for the (220) reflection is 16 (2) Å for η-alumina and 19 (2) Å for γ-alumina. The η value is slightly less than the observed thickness (20 Å) of its dehydroxylated lamellae forming perpendicular to the [111] direction of the spinel. Since the diagonal distance of the cell is $7{\cdot}9 \times \sqrt{3} = 13{\cdot}7$ Å, the stacking faults of oxygen layers from the ideal *ABCABC*... sequence along the [111] direction [*i.e.* the one-dimensional disorder suggested by Lippens & DeBoer (1964)] more likely occur between rather than within individual lamellae because each lamella is thinner than two unit cells in the d_{111} direction. Thus, the three-dimensional morphology of the pseudomorphic tablets after heating, as measured by TEM (Wefers & Misra, 1987), is the result of the relatively ordered oxygen sublattice in the long dimension and the highly disordered tetrahedral Al sublattice in the short dimension.

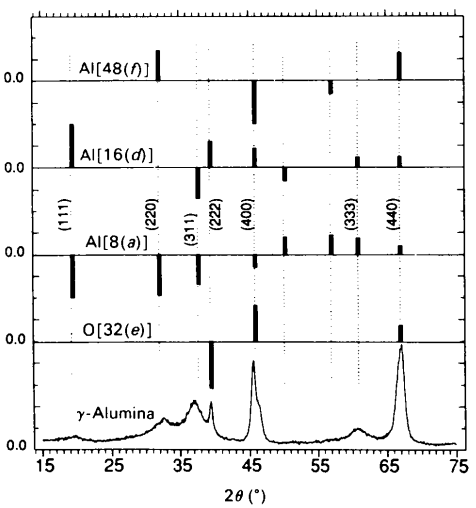

Fig. 9. XRD powder patterns of ideal spinel sublattices (negative intensity bars are of negative phase).

(*d*) The sharpest peaks are accounted for by those for which the most ordered oxygen sublattice dominates the intensity contribution. The least intense and broadest peaks are those for which the tetrahedral Al sublattice dominates. Since there is no strong diffraction intensity that is dominated by the octahedral Al sublattice in either η- or γ-alumina it must be assumed that the octahedral Al sublattice is more disordered than the oxygen sublattice but better ordered than the tetrahedral Al sublattices.

The disparity in the size of the ordering domains of the different sublattices within a single spinel lattice, which also manifests itself in the formation of odd-shaped peaks (*i.e.* sharp top with broadened base) routinely observed on the XRD powder patterns of the transition aluminas, can be understood by considering the fact that the starting hydroxides have only octahedral Al ions and quasi-cubic close-packed oxygen ions. Since the tetrahedral Al ions are the newcomers, from the dehydroxylation, they most reflect the diffusion-induced disorder.

As observed by Lippens & DeBoer (1964), γ-alumina does have a better ordered oxygen sublattice than η-alumina since its (222) reflection is sharper and stronger. However, the absence of a fairly sharp (111) reflection from γ-alumina may indicate a comparable number of tetrahedral to octahedral Al ions and possibly a better ordered tetrahedral Al sublattice in γ-alumina. This is because the (111) reflection is contributed to by the two Al sublattices which diffract out of phase, while the (220) reflection of γ-alumina, resulting only from the presence of the tetrahedral Al sublattice, is rather sharper than that of η-alumina. The results of the Rietveld structure refinement on the neutron data of η- and γ-alumina, to be presented in the following section, support these conclusions.

Rietveld refinement of η-, γ- and θ-alumina

In view of the strong profile asymmetry and extensive reflection overlapping in the XRD powder patterns of η- and γ-alumina, noted especially for the (220) and (311) reflections with relative intensities of 88 and 91%, the structure refinements were carried out on the better resolved neutron powder patterns.

In the Rietveld refinement of powder diffraction patterns (Rietveld, 1969), each point of intensity obtained from step-scanning measurements of a powder pattern is treated as a single independent observation and a profile function is introduced to

spread the calculated intensity of a reflection over the observed profile. The FWHM's of the profile function for individual reflections are allowed to vary according to a second-degree polynomial of the form

$$\mathrm{FWHM}^2 = U\tan(\theta_b)^2 + V\tan(\theta_b) + W$$

where U, V, W are empirical parameters (Caglioti, Paoletti & Ricci, 1958) to be refined in addition to the structural parameters and a background function. This UVW approach to characterizing reflection broadening is, however, not feasible for the refinement of η- and γ-alumina due to the anomalous broadening of their powder patterns. To overcome the problem, individual FWHM's of the reflections, resolved from *SHADOW* profile fitting of the η and γ patterns, were specified in the Rietveld refinement program and were kept fixed during the least-squares iterations. This is a compromise between the two-step procedure (see for example Will, Bellotto, Parrish & Hart, 1988), and the conventional Rietveld procedure where all profile parameters are refined. In the two-step procedure individual profiles are fit and then treated as single-crystal-type intensities. The problem with this procedure, which Will and others have shown to be seldom very serious, is that if any of the profile parameters correlate with any of the other Rietveld parameters then the two-step procedure is invalid as has been pointed out by Prince (1982). The compromise used here is to refine all variables in the Rietveld refinement except the FWHM's which would otherwise not be correctly modeled due to the strong anisotropy of the profiles previously discussed. This only requires the assumption that the FWHM's do not correlate with other structural parameters.

In light of the fact that the oxygen sublattice makes up more than 70% of the scattering power in the neutron patterns of η- and γ-alumina, the refinement was initiated with a trial structure model consisting of only oxygen ions located at the ideal spinel 32(*e*) site in space group *Fd3m* and allowed to converge. Fourier maps were then calculated to reveal the missing Al ions. The trial model was then updated by incorporating the newly located Al ions in the next cycle of refinement. Such an iteration procedure was carried on until all the peaks on the difference Fourier maps were resolved and identified. During the refinement, the oxygen site was kept fully occupied considering its well ordered sublattice, but no constraint was applied to the site occupancy of the Al sublattices for stoichiometry. Locally modified versions of Rietveld refinement programs *REFINE* (Prince, 1981) and *FOURIER* (Finger & Prince, 1975) were used.

The structure refinement of θ-alumina was also performed on its neutron powder pattern using the same strategy outlined for η- and γ-alumina. It was refined in space group *C2/m*. Since the monoclinic symmetry generates a substantial number of overlapping reflections that are virtually unresolvable at high angle, the last of the five segments of the pattern

Table 2. *Aluminium coordination (%) in the transition aluminas*

Form	Octahedral	Tetrahedral	Quasi-octahedral	Quasi-trihedral
Bayerite	100·0	0·000	0·000	0·000
Boehmite	100·0	0·000	0·000	0·000
η-Alumina	51 (1)	36 (1)	0·000	13 (1)
γ-Alumina	43 (1)	32 (1)	25 (1)	0·000
θ-Alumina	50 (1)	50 (1)	0·000	0·000
α-Alumina	100·0	0·000	0·000	0·000

Table 3. *Structural parameters of η-alumina*

Space group *Fd3m*, a = 7·914 (2) Å, R_b = 6·24, R_p = 6·50, R_w = 8·43%, GOF = 1·24.

Site	x	y	z	Occupancy	B (Å^2)
O 32(*e*)	0·2549 (05)	0·2549 (05)	0·2549 (05)	1·0	1·0
Al 16(*d*)	0·5000	0·5000	0·5000	0·68 (1)	0·5
Al 48(*f*)	0·3511 (54)	0·1250	0·1250	0·16 (1)	0·5
Al 32(*e*)	0·0699 (55)	0·0699 (55)	0·0699 (55)	0·09 (1)	0·5

Nearest coordination around aluminium ions

From	To	Bond distance (Å)	Multiplicity
Al[16(*d*)]	O	1·940	6
Al[48(*f*)]	O	1·641	2
Al[48(*f*)]	O	1·813	2
Al[32(*e*)]	O	1·687	3

Around	O—O spacing (Å)	Angle (°)	Multiplicity
O—Al[16(*d*)]—O	2·688	87·69	6
O—Al[16(*d*)]—O	2·799	92·31	6
O—Al[16(*d*)]—O	3·881	180·00	3
O—Al[48(*f*)]—O	2·688	95·68	1
O—Al[48(*f*)]—O	2·799	108·14	4
O—Al[48(*f*)]—O	2·908	124·72	1
O—Al[32(*e*)]—O	2·908	119·09	3

$R_b = \sum|I_o - I_c|/\sum I_o$ (Bragg R factor; I is the integrated intensity), $R_p = \sum|Y_o - Y_c|/\sum Y_o$ (pattern R factor; Y is the pattern intensity), $R_w = [\sum wt(Y_o - Y_c)^2/\sum wtY_o^2]^{1/2}$ (weighted pattern R factor).

Table 4. *Structural parameters of γ-alumina*

Space group *Fd3m*, a = 7·911 (2) Å, R_b = 10·53, R_p = 7·61, R_w = 10·25%, GOF = 1·79.

Site	x	y	z	Occupancy	B (Å^2)
O 32(*e*)	0·2547 (05)	0·2547 (05)	0·2547 (05)	1·0	1·0
Al 16(*d*)	0·5000	0·5000	0·5000	0·58 (1)	0·5
Al 8(*a*)	0·1250	0·1250	0·1250	0·84 (2)	0·5
Al 32(*e*)	0·0272 (24)	0·0272 (24)	0·0272 (24)	0·17 (2)	0·5

Nearest coordination around aluminium ions

From	To	Bond distance (Å)	Multiplicity
Al[16(*d*)]	O	1·941	6
Al[8(*a*)]	O	1·777	4
Al[32(*e*)]	O	1·835	3
Al[32(*e*)]	O	2·244	3

Around	O—O spacing (Å)	Angle (°)	Multiplicity
O—Al[16(*d*)]—O	2·692	87·78	6
O—Al[16(*d*)]—O	2.798	92·22	6
O—Al[16(*d*)]—O	3·882	180·00	3
O—Al[8(*a*)]—O	2·902	109·47	6
O—Al[32(*e*)]—O	2·902	80·57	3
O—Al[32(*e*)]—O	2·798	86·00	6
O—Al[32(*e*)]—O	2·902	104·53	3
O—Al[32(*e*)]—O	2·908	119·09	3
O—Al[32(*e*)]—O	4·031	162·34	3

Table 5. *Structural parameters of θ-alumina*

Space group $C2/m$, $a = 11{\cdot}854\ (5)$, $b = 2{\cdot}904\ (1)$, $c = 5{\cdot}622\ (2)$ Å, $\beta = 103{\cdot}83\ (7)^\circ$, $R_b = 15{\cdot}02$, $R_p = 9{\cdot}37$, $R_w = 11{\cdot}93\%$, GOF = 1·70.

Site	x	y	z	Occupancy	B (Å^2)
O_1 4(i)	0·8272 (12)	0·0000	0·4273 (44)	1·0	1·0
O_2 4(i)	0·4950 (10)	0·0000	0·2526 (19)	0·93 (4)	1·0
O_3 4(i)	0·1611 (13)	0·0000	0·0984 (45)	0·80 (2)	1·0
Al_1 4(i)	0·6595 (18)	0·0000	0·3165 (48)	0·90 (2)	0·5
Al_2 4(i)	0·9166 (15)	0·0000	0·2073 (53)	0·92 (2)	0·5

Nearest coordination around aluminium ions

From	To	Bond distance (Å)	Multiplicity
Al_1	O_2	1·896	1
Al_1	O_3	1·904	2
Al_1	O_1	1·936	1
Al_1	O_1	2·025	2
Al_2	O_2	1·710	2
Al_2	O_3	1·745	1
Al_2	O_1	1·811	1

Around	O—O spacing (Å)	Angle (°)	Multiplicity
O_1—Al_1···O_1	2·616	82·63	2
O_3—Al_1—O_1	2·637	84·26	2
O_1—Al_1—O_1	2·904	91·65	1
O_2—Al_1···O_1	2·824	92·09	2
O_3—Al_1—O_1	2·768	92·27	2
O_2—Al_1—O_3	2·748	92·64	2
O_3—Al_1—O_3	2·904	99·43	1
O_2—Al_1—O_1	3·824	172·39	1
O_3···Al_1···O_1	3·923	173·85	2
O_2—Al_2—O_1	2·822	106·51	2
O_2—Al_2—O_3	2·771	106·66	2
O_3—Al_2—O_1	2·992	114·54	1
O_2—Al_2—O_2	2·904	116·25	1

Table 6. *Reflection list of η-alumina*

The last four columns are structure-factor components from individual sublattices of the structure and add up to F.

h	k	l	d (Å)	I_o (%)	I_c (%)	F	O[32(e)]	Al[16(d)]	Al[48(f)]	Al[32(e)]
1	1	1	4·5692	3·6	4·1	0·51	0·21	0·54	0·08	−0·16
2	2	0	2·7981	0·0	0·0	0·05	−0·02	0·00	0·22	−0·15
3	1	1	2·3862	5·4	4·1	−0·50	0·07	−0·53	0·02	−0·06
2	2	2	2·2846	56·1	54·7	−3·29	−4·40	1·05	0·00	0·07
4	0	0	1·9785	61·5	62·0	4·65	4·32	1·04	0·67	−0·05
3	3	1	1·8156	0·8	0·3	0·22	0·33	−0·52	−0·12	0·09
4	2	2	1·6155	0·2	0·3	0·24	−0·02	0·00	0·25	0·03
3	3	3	1·5231	0·3	0·3	0·36	−0·57	0·51	0·21	−0·09
5	1	1	1·5231	8·2	8·2	1·11	0·45	0·51	0·16	0·00
4	4	0	1·3990	100·0	100·0	5·65	4·03	1·01	0·61	0·01
5	3	1	1·3377	3·8	3·4	−0·68	0·18	0·50	0·06	−0·06
4	4	2	1·3190	0·0	0·0	−0·09	0·06	0·00	0·00	−0·15
6	2	0	1·2513	0·7	0·2	−0·26	0·04	0·00	−0·13	0·09
5	3	3	1·2069	1·3	0·9	−0·52	0·06	0·49	0·03	−0·12
6	2	2	1·1931	39·3	40·5	−2·91	−3·82	0·99	0·00	−0·08
4	4	4	1·1423	27·4	27·1	4·18	3·75	0·98	−0·55	0·00
5	5	1	1·1082	0·9	1·9	0·83	0·63	0·49	−0·24	0·06
7	1	1	1·1082	0·2	0·5	−0·40	0·29	0·49	−0·09	−0·12
6	4	2	1·0576	1·1	0·1	0·14	0·04	0·00	0·16	0·02
7	3	1	1·0303	0·3	0·3	0·23	0·50	−0·48	0·18	0·03
5	5	3	1·0303	2·7	2·7	−0·87	0·38	0·48	−0·14	0·13
8	0	0	0·9893	19·1	20·8	4·73	3·49	0·95	0·51	−0·21
7	3	3	0·9669	0·6	0·1	0·14	−0·70	0·47	0·26	0·11
6	4	4	0·9597	1·1	0·1	0·24	0·05	0·00	0·00	0·19
8	2	2	0·9327	0·9	0·5	0·44	−0·01	0·00	0·33	0·12
6	6	0	0·9327	0·0	0·0	−0·12	−0·12	0·00	0·05	−0·05
7	5	1	0·9138	0·9	0·6	−0·38	0·06	−0·46	0·01	0·02
5	5	5	0·9138	3·9	2·7	1·70	0·78	0·46	0·30	0·15
6	6	2	0·9078	7·4	8·1	−2·27	−3·31	0·92	0·00	0·11

(collected from five detectors simultaneously) was truncated from the refinement. The total number of reflections was reduced from 155 to 108.

The results are listed in Tables 2–8 and illustrated in Fig. 7. As an additional test of the validity of the three refined structures, the total number of Al ions

Table 7. *Reflection list of γ-alumina*

h	k	l	d (Å)	I_o (%)	I_c (%)	F	O[32(e)]	Al[16(d)]	Al[8(a)]	Al[32(e)]
1	1	1	4·5672	0·0	0·0	−0·03	0·20	0·41	−0·40	−0·24
2	2	0	2·7969	1·7	2·3	−0·63	−0·02	0·00	−0·56	−0·05
3	1	1	2·3852	3·6	4·2	−0·57	0·07	−0·40	−0·40	0·16
2	2	2	2·2836	60·0	59·9	−3·23	−4·40	0·80	0·00	0·38
4	0	0	1·9777	63·9	68·4	4·91	4·33	0·79	−0·55	0·35
3	3	1	1·8148	1·0	1·3	0·50	0·31	−0·39	0·39	0·19
4	2	2	1·6148	1·0	1·0	0·49	−0·01	0·00	0·55	−0·04
3	3	3	1·5224	0·0	0·0	−0·06	−0·55	0·39	0·38	−0·28
5	1	1	1·5224	4·8	4·9	1·00	0·43	0·39	0·38	−0·20
4	4	0	1·3984	100·0	100·0	5·60	4·03	0·77	0·54	0·26
5	3	1	1·3372	1·8	0·1	−0·13	−0·18	−0·38	0·38	0·06
4	4	2	1·3185	1·3	0·0	−0·11	0·06	0·00	0·00	−0·16
6	2	0	1·2508	1·4	0·4	0·37	−0·04	0·00	0·53	−0·12
5	3	3	1·2064	3·9	1·3	−0·69	0·05	−0·38	0·37	0·00
6	2	2	1·1926	33·4	34·6	−2·88	−3·82	0·75	0·00	0·20
4	4	4	1·1418	25·8	29·2	4·18	3·75	0·74	−0·52	0·20
5	5	1	1·1077	0·3	0·3	0·37	0·60	0·37	−0·37	−0·24
7	1	1	1·1077	0·2	0·2	0·28	0·28	−0·37	0·37	0·01
6	4	2	1·0571	1·0	1·9	−0·64	−0·04	0·00	−0·51	0·09
7	3	1	1·0299	0·0	0·1	−0·12	0·48	−0·36	−0·36	0·12
5	5	3	1·0299	1·4	2·4	−1·01	−0·37	−0·36	−0·36	0·08
8	0	0	0·9888	13·1	15·8	4·81	3·50	0·72	0·50	0·08
7	3	3	0·9664	3·2	1·8	−0·90	−0·67	0·36	−0·35	−0·23
6	4	4	0·9593	0·0	0·0	−0·04	0·05	0·00	0·00	−0·08
8	2	2	0·9323	0·2	0·6	−0·52	−0·01	0·00	0·50	−0·01
6	6	0	0·9323	0·4	0·9	−0·89	0·11	0·00	−0·50	−0·29
7	5	1	0·9134	3·2	2·1	−0·75	0·05	−0·35	0·35	−0·10
5	5	5	0·9134	1·6	1·0	1·17	0·75	0·35	0·35	−0·28
6	6	2	0·9074	5·5	7·0	−2·51	3·32	0·70	0·00	0·10

Table 8. *Reflection list of θ-alumina*

Only reflections with the 30 highest relative intensities are listed.

h	k	l	d (Å)	I_o (%)	I_c (%)	F	O_1	O_2	O_3	Al_1	Al_2
0	0	1	5·4591	6·0	5·8	−0·38	−1·03	−0·02	0·75	−0·24	0·16
4	0	1	2·8412	12·2	11·7	−1·02	0·83	0·15	−0·87	−0·26	−0·58
−2	0	2	2·7321	6·6	6·9	0·82	0·35	−1·04	0·64	0·23	−0·52
0	0	2	2·7295	9·4	9·8	0·98	0·69	−1·05	0·30	0·40	0·51
1	1	1	2·4451	12·6	14·3	0·91	−0·03	−0·02	−0·05	0·58	0·42
4	0	1	2·3265	7·1	6·9	0·96	0·10	0·11	−0·04	0·56	0·42
3	1	0	2·3157	91·6	88·9	−2·43	−1·10	−1·03	−0·88	0·58	0·00
−4	0	2	2·2698	42·7	39·6	2·34	−1·06	−1·02	0·84	0·59	−0·01
2	0	2	2·2654	46·2	43·1	−2·45	−1·10	1·03	−0·88	0·56	0·01
1	1	2	2·0199	100·0	100·0	2·93	1·08	1·02	0·85	0·58	−0·59
−6	0	1	1·9626	17·8	8·0	1·20	1·06	−0·21	0·59	−0·37	−0·16
6	0	0	1·9184	39·7	43·6	2·88	1·06	1·00	0·85	0·56	0·59
4	0	3	1·7370	6·9	5·0	1·07	1·05	0·17	0·50	−0·22	0·56
3	1	3	1·5431	17·3	15·2	1·47	0·32	−0·14	0·32	0·56	0·40
1	1	3	1·4892	9·5	6·8	−1·01	0·80	0·02	−0·80	−0·44	−0·56
8	0	1	1·4813	8·6	6·3	1·38	0·38	−0·26	0·30	0·55	0·41
0	2	0	1·4521	45·0	50·0	3·96	1·03	0·96	0·83	0·57	0·57
7	1	0	1·4309	11·7	6·5	1·02	0·26	0·94	0·57	−0·42	0·50
−2	0	4	1·4055	53·4	42·2	3·76	0·96	0·95	0·74	0·53	0·57
7	1	2	1·3920	90·8	82·6	3·74	0·94	0·92	0·74	0·56	0·57
5	1	2	1·3900	96·8	88·0	3·86	1·02	0·95	0·82	0·51	0·57
−4	2	2	1·2232	16·8	19·7	−2·05	−0·94	0·91	−0·75	0·55	−0·01
2	2	2	1·2225	18·3	21·7	−2·14	0·98	−0·92	−0·78	0·53	0·01
5	1	4	1·2022	17·9	16·1	1·88	−0·88	0·89	0·67	0·54	0·01
1	1	4	1·2009	23·7	20·5	−2·12	−0·95	0·91	−0·74	0·49	−0·01
9	1	0	1·1705	17·0	17·6	2·01	−0·91	0·87	−0·74	0·51	0·00
8	0	2	1·1632	10·2	10·0	−2·15	0·95	0·88	−0·77	0·46	−0·01
6	2	0	1·1578	38·2	28·1	2·55	0·94	0·88	0·76	0·53	−0·55
8	0	4	1·1349	14·8	10·5	2·25	0·80	0·85	0·61	0·55	−0·55
4	0	4	1·1327	15·9	12·8	2·48	0·95	0·89	0·74	0·45	0·55

was also refined and for each structure it converged to within two standard deviations of the ideal 2:3 ratio required by the formula Al_2O_3. This is despite the absence of any chemical constraints in the refinements. As a result the values of the Al site occupancy listed in Tables 2, 3, 4 and 5 have been normalized to the ideal 2:3.

No residual OH's and OD's were found in the three refined structures. This finding is consistent

with the combined results of the loss-on-ignition analysis and statistical analysis of the significance threshold for the Fourier synthesis on the three structures. The background of the scattering density at the 3σ level on the Fourier map from the final cycle of refinement is 3·0, 6·0 and 12·0% for η-, γ- and θ-alumina respectively. If the residual OH's and OD's were well ordered in the structures, these numbers should translate approximately to detectability levels of about 1·2, 1·6 and 1·5 wt% in loss-on-ignition for η-, γ- and θ-alumina respectively.

The refinement results show that Al ions in η-alumina occupy only one octahedral site [16(*d*)], one tetrahedral site [48(*f*)], and one *quasi-trihedral* site [32(*e*)]. These results disagree substantially with those of the X-ray refinement by Shirasuka, Yanagida & Yamaguchi (1976). The disagreement mainly lies in the absence of Al ions at tetrahedral site [8(*a*)] and the presence of quasi-trihedral Al ions.

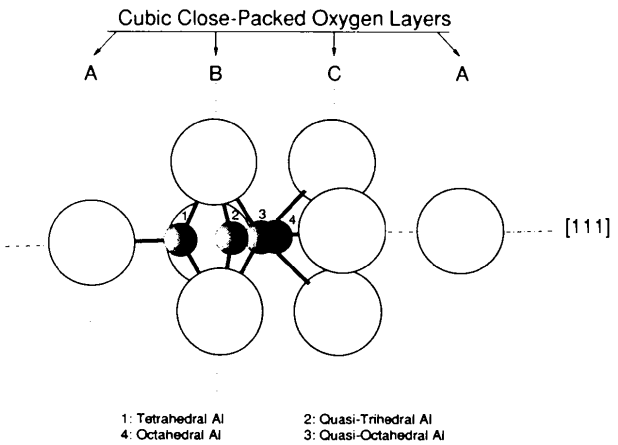

Fig. 10. Aluminium coordination in the transitiom aluminas.

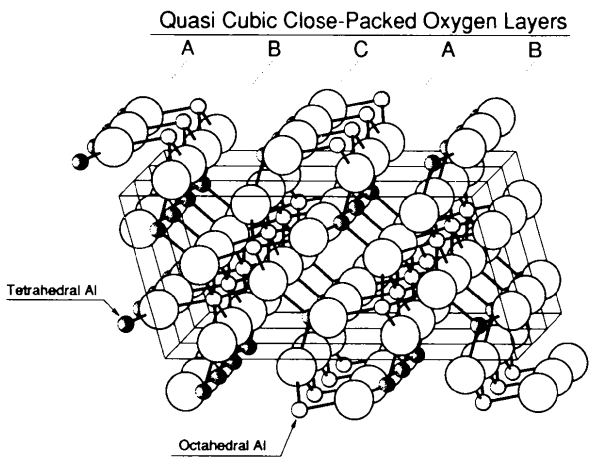

Fig. 11. Crystal structure of θ-alumina.

The quasi-trihedral Al ions are slightly displaced (0·162 Å) away from the oxygen plane toward the second octahedral site [16(*c*)] [0·958 Å away from site 16(*c*), see Fig. 10]. In γ-alumina, however, Al ions occupy only one octahedral site [16(*d*)], one tetrahedral site [8(*a*)], and one *quasi-octahedral* site [32(*e*)]. The quasi-octahedral Al ions are 0·373 Å away from the octahedral site [16(*c*)] and 0·748 Å away from the nearest oxygen plane. The extraordinary presence of nearly pure three-coordinated Al ions in η-alumina and of the quasi-octahedral Al ions in γ-alumina will be discussed later on.

In θ-alumina, Al ions occupy only one octahedral site and one tetrahedral site. Notice that most of the sites including those of oxygen are not fully occupied. This is nevertheless consistent with the metastable nature of this transition form. The structure of θ-alumina can also be viewed as a distorted spinel lattice (see Fig. 11). Tetrahedral and octahedral Al ions are seen to be filling alternating spaces between oxygen layers stacking in the [$\bar{2}$01] direction, which happens to be the same direction as the spinel [111]! Fig. 2 supports this finding where the (111) reflection of η-alumina persists with increasing calcination temperature and becomes the ($\bar{2}$01) reflection of θ-alumina. Therefore, the average interplanar spacing of the cubic close-packed oxygen ions in the θ structure is $d_{\bar{4}02} = 2{\cdot}266\ (1)$ Å.

Discussion

Effects of surface energy on the structures of η- and γ-alumina: the presence of quasi-three- and six-coordinated aluminium ions

Since the Al ion favors octahedral coordination under normal circumstances, the high surface area/energy must be the cause for the presence of quasi-trihedral Al ions in η-alumina and the quasi-octahedral Al ions in γ-alumina. We propose that these extraordinary abnormally coordinated Al ions are located in the surface layer. As dehydroxylation proceeds, newly formed surfaces with exposed bond-ruptured Al ions are created, which are in a very unstable high-energy state. To reduce the surface energy, the more polarizable oxygen anions in the newly created surface layer will become polarized resulting in a relative displacement between the surface oxygen anions and Al cation layers along the (111) planes of the spinel [since most of the new surfaces are spinel (111) planes]. The greater the surface polarization and displacement, the lower the residual surface energy. Quasi-trihedral Al ions are therefore found in η-alumina and quasi-octahedral Al ions in γ-alumina because η, derived from bayerite, has a much higher specific surface area, and presumably higher residual surface energy, than γ

which is derived from boehmite. These abnormally coordinated Al cations are obviously responsible for the strong Lewis acidity (electron-acceptor property) observed on the surfaces of η- and γ-alumina (Tamele, 1950; Milliken, Mills & Oblad, 1950) and clearly must result in the catalytic activity of these phases. The above conclusion is also supported by the following evidence:

(*a*) The refined number of quasi-trihedral Al ions in η-alumina is 13 (1)% of the total or 0·026 (1) sites $Å^{-2}$ on the (111) surface of the spinel [see Fig. 12, and notice that a maximum of 0·04 sites $Å^{-2}$ can be fit onto the (111) surface]. This agrees reasonably well with:

(i) The statistical percentage of atoms in the surface layer, which can be estimated from the value of the specific area. A typical value for the specific surface area of η-alumina is 300 $m^2 g^{-1}$ or $3·0 \times 10^6$ $cm^2 g^{-1}$ and bulk density 3·65 g cm^{-3}. Assuming 1·2 Å thickness of the surface layer, then

$$\text{Surface/bulk volume} = 3·0 \times 10^6 \times 1·2 \times 10^{-8} \times 3·65 = 13\%.$$

This extremely high percentage explains why the neutron diffraction experiment 'saw' the unusually coordinated surface atoms.

(ii) The number of possible surface Lewis acid sites derived from surface adsorption data: 0·02 sites $Å^{-2}$ on γ-alumina (Cornelius, Milliken, Mills & Oblad, 1966); 0·03 sites $Å^{-2}$ on η-alumina (Peri, 1965).

The small discrepancy may easily be accounted for by minor differences in sample preparation, by the difficulty in exactly differentiating chemisorption from the physisorption stage, by small deviations in the measurement of surface area, and/or by the fact that some of the surfaces are not the (111) planes of the spinel structure. Considering these factors, our observed value of 0·026 (1) sites $Å^{-2}$ in η-alumina is in very good agreement with these reports.

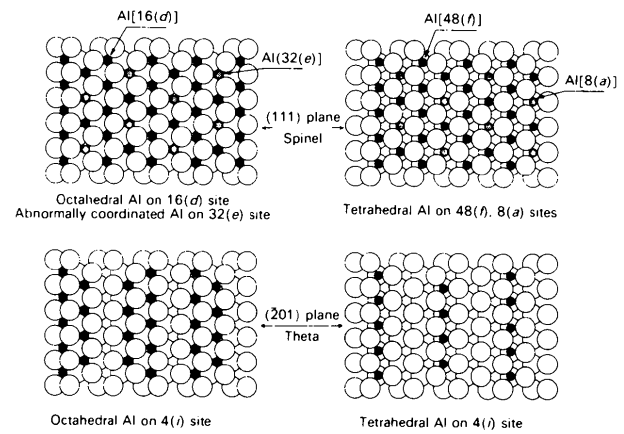

Fig. 12. Site occupation by Al ions in η-, γ- and θ-alumina.

(*b*) The oxygen ions in both η- and γ-alumina are displaced by 0·07 (1) Å along the diagonal [111] direction away from the ideal spinel position. The Al–O polyhedra are rather distorted in the transition aluminas. The average Al—O bond length of the octahedra in η-, γ- and θ-alumina varies from 1·94 to 1·95 Å, much longer than the 1·90–1·91 Å range found in α-alumina, bayerite and boehmite. The average interplanar spacing of cubic close-packed oxygen ions is 2·282 (1) Å in η- and γ-alumina, and 2·266 (1) Å in θ-alumina; both are much longer than the 2·165 (1) Å in α-alumina. These structural differences can be accounted for by the displacement of surface oxygen layers in light of the fact that the observed lamellae in the transition aluminas are not much thicker than the diagonal distance of a single spinel cell.

It must be pointed out that the quasi-octahedral Al ions in γ-alumina may not be all catalytically active in view of their pronounced displacement away from the surface oxygen layer into the bulk. Crystallographically, a maximum of 0·04 sites $Å^{-2}$ surface or 18·75% of the Al ions can be accommodated in the (111) surface layer of the spinel (see Fig. 12). It is also recognized, from the pseudomorphosis of dehydroxylation of boehmite, that a substantial portion of the surface area in γ-alumina comes from less-densely packed crystal planes other than the (111). Therefore, the 25% quasi-octahedral Al ions (equivalent to 0·05 sites $Å^{-2}$ surface) is too high to be all in the surface. Since neutron diffraction mainly sees the nuclear lattice of the structure, the exact electronic environment around the quasi-octahedral Al cations could be very different from the viewpoint of chemical reactivity. Therefore, no attempt has been made to correlate the 25% value to the available experimental data of surface adsorption carried out on γ-alumina.

Structural differences between η- and γ-alumina

In addition to the above differences, tetrahedral Al ions in η-alumina are all in the 48-fold site, presumably very disordered since the site occupancy is only 16%, whereas those in γ-alumina are all in the 8-fold sites, presumably much better ordered since the site occupancy is 84%. However, the fraction of octahedral Al ions without counting the surface Al ions is 51 (1) and 43 (1)% in η- and γ-alumina respectively. These numbers are very close to the 50% value in θ-alumina but much lower than the 65–70% range determined by Shirasuka, Yanagida & Yamaguchi (1976) from XRD powder analysis and by John, Alma & Hays (1983) from solid-state NMR. This discrepancy apparently lies in the presence of the surface Al cations around which the oxygen anions are more or less polarized making

them look octahedrally coordinated under XRD and NMR. In other words, XRD and NMR cannot distinguish surface Al ions from those in the bulk. The inevitable cation vacancies in the spinel thus appear to slightly favor octahedral sites in η-alumina but tetrahedral sites in γ-alumina.

The site occupancy of the octahedral and tetrahedral Al ions in the defect spinel lattice of η- and γ-alumina is such that Al ions mainly fill the alternating spaces between the cubic close-packed oxygen layers (see Fig. 8). This kind of order is unexpected if one considers the chaotic nature of the dehydroxylation and the extent of structural rearrangement which must be undertaken when 50% (in bayerite) and 25% (in boehmite) of the oxygen ions leave to form η- and γ-alumina.

In order to study the role of the unusually coordinated surface Al ions in determining the symmetry of η- and γ-alumina, samples of η- and γ-alumina were mixed with less than 1·0% of finely ground sodium chloride and fired. While pure η- and γ-alumina exhibit more pronounced tetragonal character when heated to higher temperatures (see Figs. 2 and 3), the η- and γ-alumina doped with sodium chloride show virtually no sign of further tetragonal deformation up to 1373 K (see Fig. 13). The transition to θ-alumina is completely suppressed in the doped samples. This result can be explained by assuming that the large sodium ions take up surface octahedral sites and hinder the diffusion of surface Al ions to the orderly tetrahedral sites which are apparently needed for η- an γ-alumina to transform into θ-alumina. This suggests that the tetragonal 'deformation' in η- and γ-aluminas is caused mainly by the ordering of tetrahedral Al sublattices in the structures. γ-Alumina with its better ordered tetrahedral Al sublattice thus exhibits more pronounced tetragonal character than η-alumina, while θ-alumina with its well ordered tetrahedral Al sublattice has already turned into the monoclinic form. On this basis, the overall crystal structure of the transition aluminas must not be taken intrinsically as *tetragonally deformed* but as *spinel deformed* in that they are deformed *into* not out of the spinel structure.

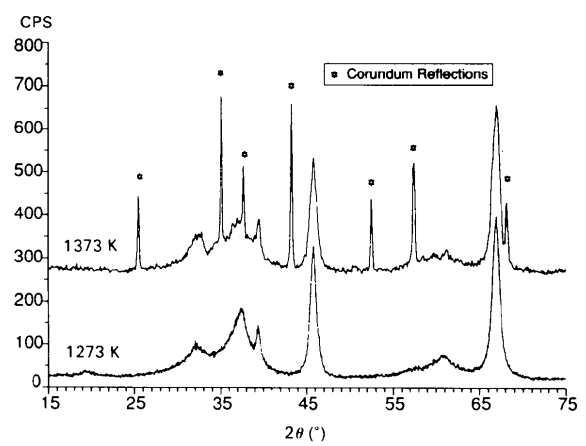

Fig. 13. XRD scans of η-alumina doped with < 1·0 wt% NaCl.

Transition of η- and γ- to θ-alumina

The fact that all three transition forms have similar *ABCABC*... stacking of cubic close-packed oxygen ions suggests that the transition of η- or γ- to θ-alumina need not be a reconstructive recrystallization process as concluded by Lippens & DeBoer (1964). Instead it should be a displacive one in which the structure increases its order by aligning and merging the lamellae thereby reducing internal pores and surfaces as well as the stacking faults in the [111] direction; and by diffusion of the surface Al ions to more-ordered sites. This conclusion is supported by the following evidence:

(*a*) All three structures have about 50/50 octahedral and tetrahedral Al ions. The phenomenon of alternating layers filled by octahedral and tetrahedral Al ions is common to the three structures. Fig. 12 illustrates the site distribution of the different coordinated Al ions in the (111) plane of the η and γ lattices as well as in the (2̄01) plane of the θ lattice. Notice the similarity of the octahedral sites among the three structures. In comparison, the poorly occupied 48-fold tetrahedral site of η-alumina, in both distribution and population, approaches the 4-fold tetrahedral site of θ-alumina more than the well occupied 8-fold tetrahedral site of γ-alumina does. This may explain why a higher temperature (see Figs. 2 and 3) is required for γ-alumina to transform into θ-alumina and into corundum despite its oxygen sublattice being better ordered than that of η-alumina.

(*b*) Doping η- and γ-alumina with traces of sodium chloride completely suppressed the transition to θ-alumina. The doped η- and γ-alumina can maintain their defect spinel lattice up to 1373 K above which the oxygen ions are sufficiently activated to diffuse so as to break up the *ABCABC*... cubic close-packed oxygen layers and thus to allow for the recrystallization of corundum with its oxygen ions in the hexagonally close-packed *ABABAB*... arrangement.

(*c*) The (111) reflection of η-alumina persists with increasing temperature and becomes the strong (2̄01) reflection of θ-alumina, both of which belong to the same crystal zone of the spinel lattice. However, the XRD powder pattern of θ-alumina shows no single reflection that is significantly sharper than the (222) reflections of η- or γ-alumina. The ordering domain

sizes of the oxygen sublattices in the three structures are comparable.

(*d*) A distinctive coexistence of η- or γ- with θ-alumina in an XRD pattern has not yet been seen. This should normally accompany a reconstructive recrystallization as shown in Fig. 13. Instead we routinely see a gradual sharpening and splitting of the diffraction patterns as η- and γ-alumina transform into θ-alumina.

(*e*) DTA data show neither endothermic nor exothermic activity in the temperature region during which the transition of η- or γ- to θ-alumina takes place.

Concluding remarks

A summary of the conclusions from this work are:

(*a*) Residual hydroxyl ions in the transition aluminas, as established by weight loss, are less than had previously been thought.

(*b*) The persistence of the oxygen framework from the hydroxides, as measured from zonal XRD profile broadening, accounts for the pseudomorphis of the η or γ transitions.

(*c*) The complete tablet morphology after the transformation, the three-dimensional morphology of the pseudomorphic tablets after heating, as measured by TEM (Wefers & Misra, 1987), is the result of the relatively ordered oxygen sublattice in the long dimension and the highly disorderd tetrahedral aluminium sublattice in the short dimension.

(*d*) The formation of odd-shaped peaks, which are routinely observed in the XRD powder patterns of the transition aluminas, is the manifestation of the disparity in the size of ordering domains of different sublattices within their defect spinel framework. In addition, some of the anomalous peak asymmetry in the η-alumina pattern is due to the inevitable presence of some γ-alumina impurity (*i.e.* two different tetraheral ordering lengths producing a peak composed of two different size-broadened profiles). This may be the result of the different dimensions in the tablet morphology.

(*e*) The presence of a nearly pure three-coordinated Al ion in η-alumina shows the extraordinary role that surface energy plays in the free energy of stabilization of this phase and certainly has implications for the observed catalytic activity.

(*f*) The abnormally coordinated Al cations are responsible for the strong Lewis acidity (electron-acceptor property) observed on the surfaces of η- and γ-alumina (Tamele, 1950; Milliken, Mills & Oblad, 1950) and must result in the catalytic activity of these phases.

(*g*) The transition of η- or γ- to θ-alumina is not a reconstructive recrystallization process as previously thought, but a displacive one in which the ordering of the tetrahedral Al sublattice mainly causes the spinel symmetry to collapse so that the structure, which exhibits tetragonal character at the early stage of the transition, settles into monoclinic θ-alumina at the later stage. The overall crystal structure of the transition aluminas should therefore be viewed intrinsically as *spinel deformed* rather than as *tetragonally deformed.*

The initial phases of this work were supported by the Alcoa Corporation and the authors are particularly indebted to Dr Karl Wefers for his encouragement. The neutron powder data were collected at the National Institute of Science and Technology by Dr E. E. Prince whose help was invaluable. The New York State College of Ceramics and the New York State Science and Technology Foundations's Center for Advanced Ceramic Technology are thanked for their support.

References

CAGLIOTI, G., PAOLETTI, A. & RICCI, F. P. (1958). *Nucl. Instrum.* **3**, 223–228.

CORNELIUS, E. B., MILLIKEN, T. H., MILLS, G. A. & OBLAD, A. G. (1955). *J. Phys. Chem.* **59**, 10–14, 809–813.

DEBOER, J. H. & HOUBEN, G. M. M. (1952). *Proceedings of the International Symposium on the Reactivity of Solids*, Part I, pp. 237–244. Göteborg, Flanders Boktryckeri Aktieboolag.

ERVIN, G. JR (1952). *Acta Cryst.* **5**, 103–108.

FINGER, L. W. & PRINCE, E. E. (1975). *Natl Bur. Stand. (US) Tech. Note* 854.

GOTON, R. (1955). Thesis, Univ. of Lyon, France.

HILL, R. J. (1981). *Clays Clay Miner.* **29**(6), 435–445.

HOWARD, S. A. & SNYDER, R. L. (1985). *Advances in Materials Characterization*, Vol. II, edited by R. L. SNYDER, R. A. CONDRATE & P. F. JOHNSON, pp. 57–71. New York: Plenum.

HOWARD, S. A. & SNYDER, R. L. (1989). *J. Appl. Cryst.* **22**, 238–243.

JOHN, C. S., ALMA, V. C. M. & HAYS, G. R. (1983). *Appl. Catal.* **6**, 341–346.

KORDES, E. (1935). *Z. Kristallogr.* **91**, 193–228.

LIPPENS, B. C. (1961). Thesis, Technical Univ. Delft, The Netherlands.

LIPPENS, B. C. & DEBOER, J. H. (1964). *Acta Cryst.* **17**, 1312–1321.

MILLIKEN, T. H., MILLS, G. A. & OBLAD, A. G. (1950). *Discuss. Faraday Soc.* **8**, 279–290.

PERI, J. B. (1965). *J. Phys. Chem.* **69**, 231–239.

PRINCE, E. (1981). *J. Appl. Cryst.* **14**, 157–159.

PRINCE, E. (1982). *Natl Bur. Stand. (US) Tech. Note.*

RIETVELD, H. M. (1969). *J. Appl. Cryst.* **2**, 65–71.

SAALFELD, H. (1960). *Neues Jahrb. Mineral. Abh.* **95**, 1–87.

SAALFELD, H. & MEHROTRA, B. (1965). *Ber. Dtsch. Keram. Ges.* **42**, 161–166.

SCHERRER, P. (1918). *Gött. Nachr.* **2**, 98.

SHIRASUKA, K., YANAGIDA, H. & YAMAGUCHI, G. (1976). *Yogyo Kyokai Shi*, **84**(12), 610–613.

SOLED, S. (1983). *J. Catal.* **81**, 252–257.

STUMPF, H. C., RUSSELL, A. S., NEWSOME, J. W. & TUCKER, C. M. (1950). *Ind. Eng. Chem.* **42**, 1398–1403.

TAMELE, M. W. (1950). *Discuss. Faraday Soc.* **8**, 270–279.

WEFERS, K. & MISRA, C. (1987). Alcoa Technical Paper No. 19, revised. Alcoa Laboratories, Pittsburg, PA, USA.

WILL, G., BELLOTTO, M., PARRISH, W. & HART, M. (1988). *J. Appl. Cryst.* **21**, 182–191.

YAMAGUCHI, G. & YANAGIDA, H. (1964). *Bull. Chem. Soc. Jpn*, **38**, 1229–1231.
YAMAGUCHI, G., YANAGIDA, H. & ONO, S. (1964). *Bull. Chem. Soc. Jpn*, **37**, 752–754, 1555–1557.
YAMAGUCHI, G., YASUI, I. & CHIU, W. (1970). *Bull. Chem. Soc. Jpn*, **43**, 2487–2491.
ZIGAN, F., JOSWIG, W. & BURGER, N. (1978). *Z. Kristallogr.* **148**, 255–273.

Acta Cryst. (1991). B**47**, 630–634

Refinement of Structures of the Composite Crystals $Ba_xFe_2S_4$ (x = 10/9 and 9/8) in a Four-Dimensional Formalism

BY MITSUKO ONODA AND KATSUO KATO

National Institute for Research in Inorganic Materials, 1-1 *Namiki, Tsukuba, Ibaraki* 305, *Japan*

(*Received* 8 *August* 1990; *accepted* 6 *March* 1991)

Abstract

The structures of the composite crystals of tetragonal columnar sulfide, $Ba_{10/9}Fe_2S_4$ (M_r = 392·55) and $Ba_{9/8}Fe_2S_4$ (M_r = 394·46), have been refined on the basis of a four-dimensional superspace group using the X-ray diffraction data collected by Grey [*Acta Cryst.* (1975), B**31**, 45–48] and Hoggins & Steinfink [*Acta Cryst.* (1977), B**33**, 673–678]. The crystals are composed of linear strings of edge-shared FeS_4 tetrahedra $(FeS_{4/2})_\infty$ and rows of Ba ions. R_F was 0·082 on a commensurate modulated structure model with 23 structural parameters using 212 reflections for $Ba_{10/9}Fe_2S_4$, and 0·153 with 33 parameters using 1083 reflections for $Ba_{9/8}Fe_2S_4$. The symmetry operations of the superspace group employed are $(0,0,0,0;\ \frac{1}{2},\frac{1}{2},\frac{1}{2},\frac{1}{2}) + x_1,x_2,x_3,x_4;\ -x_2,x_1,x_3,x_4;\ -x_1,x_2,\frac{1}{2} + x_3,x_4;\ x_2,x_1,\frac{1}{2} + x_3,x_4;\ -x_1,-x_2,x_3,x_4;\ x_2,-x_1,x_3,x_4;\ x_1,-x_2,\frac{1}{2} + x_3,x_4;\ -x_2,-x_1,\frac{1}{2} + x_3,x_4$, and the superspace group can be transformed into P^{I4bm}_{1ss} with a basis transformation. The unit cells and other crystal data are $a_1 = a_2 = 7{\cdot}776$, $a_3 = 5{\cdot}540$ Å, $\sigma = (0\,0\,10/9)$, $V = 334{\cdot}98$ Å^3, $D_x = 3{\cdot}89$ Mg m^{-3}, $Z = 2$ for $Ba_{10/9}Fe_2S_4$, and $a_1 = a_2 = 7{\cdot}776$, $a_3 = 5{\cdot}551$ Å, $\sigma = (0\,0\,9/8)$, $V = 334{\cdot}10$ Å^3, $D_x = 3{\cdot}90$ Mg m^{-3}, $Z = 2$ for $Ba_{9/8}Fe_2S_4$.

Introduction

Recently, it has become clear that some crystals consist of plural structural units, each with its own periodicity (Janner & Janssen, 1980; Makovicky & Hyde, 1981), and they are called composite crystals (Janner & Janssen, 1980). Layered ternary chalcogenides such as $(LaS)_{1.2}CrS_2$ with composite crystal structures have attracted much interest (Kato, Kawada & Takahashi, 1977; Wiegers, Meetsma, van Smaalen, Haange, Wulff, Zeinstra, de Boer, Kuypers, van Tendeloo, van Landuyt, Amelinckx, Meerschaut, Rabu & Rouxel, 1989; Kato, 1990; Onoda, Kato, Gotoh & Oosawa, 1990). These crystal structures have been described as an interpenetration of two layered structures which alternate regularly through the crystal in spite of the misfit between their two-dimensional lattices. The description of such a total structure can be based on superspace-group theory (Janner & Janssen, 1980).

The present paper is concerned with columnar composite structures. Examples such as $Ba_xFe_2S_4$ (x = 10/9 and 9/8) (Grey, 1975; Hoggins & Steinfink, 1977) and $A_{1-x}Cr_2X_{4-x}$ (A = Eu, Sr, Ba, Pb; X = S, Se; x = 0·29) (Brouwer & Jellinek, 1977; Brouwer, 1978) are found among the ternary chalcogenides.

The columnar-compound series $Ba_xFe_2S_4$ (1·00 ≤ x ≤ 1·142) have been intensively investigated by X-ray diffraction (Grey, 1974, 1975; Hoggins & Steinfink, 1977; Boller, 1978; Swinnea & Steinfink, 1980, 1982*a*; Nakayama, Kosuge & Kachi, 1981), electron diffraction, electron microscopy (Nakayama, Kosuge & Kachi, 1980, 1982; Holladay & Eyring, 1986) and measurement of physical properties (Swinnea & Steinfink, 1982*b*). The crystal structures of $Ba_{10/9}Fe_2S_4$ (Grey, 1975) and $Ba_{9/8}Fe_2S_4$ (Hoggins & Steinfink, 1977) have been determined by a single-crystal X-ray analysis and refined with the superstructure model. The crystals are tetragonal with a = 7·776 and c = 49·86 Å for $Ba_{10/9}Fe_2S_4$, and a = 7·776 and c = 44·41 Å for $Ba_{9/8}Fe_2S_4$. Their structures consist of chains of edge-shared Fe–S tetrahedra, $(FeS_{4/2})_\infty$, along [001]; the Ba atoms are packed between the chains with a linear density of more than one atom within the basic period of the latter.

The diffraction intensity data of $Ba_{10/9}Fe_2S_4$ and $Ba_{9/8}Fe_2S_4$ seem to exhibit many absences not related to space-group extinctions. Diffractions which are very weak or absent can be indexed as higher-order

0108-7681/91/050630-05$03.00